Low-temperature and high-pressure μSR study of the strongly correlated $CeNiSnH_x$ compounds

O. Isnard,[1,2] C. Rusu,[3] R. Dudric,[3] D. Andreica,[3] A. Amato,[4] and B. Chevalier[5]
[1]*Université Grenoble Alpes, Institut Néel, F-38042 Grenoble, France*
[2]*CNRS, Institut Néel, 25 Rue des Martyrs, F-38042 Grenoble, France*
[3]*Faculty of Physics, Babeş-Bolyai University, RO-400084 Cluj Napoca, Romania*
[4]*Laboratory for Muon Spin Spectroscopy, Paul Scherrer Institut, CH-5232 Villigen-PSI, Switzerland*
[5]*CNRS, Université Bordeaux, ICMCB, UPR 9048, F-33600 Pessac, France*
(Received 14 March 2016; revised manuscript received 3 May 2016; published 23 June 2016)

Hydrogen insertion in the CeNiSn Kondo semiconductor induces antiferromagnetic ordering for CeNiSnH below $T_N = 4.5$ K whereas $CeNiSnH_{1.8}$ orders ferromagnetically below $T_C = 7.0$ K. We present a detailed investigation of these $CeNiSnH_x$ compounds by means of muon spin spectroscopy performed at both ambient and high pressure (up to 23 kbar). It is shown that both magnetic ordering temperatures are sensitive to the applied pressure but in opposite directions, i.e., $\frac{dT_C}{dp} = -0.17\ \mathrm{K\,kbar^{-1}}$ for $CeNiSnH_{1.8}$ and $\frac{dT_N}{dp} = 0.016\ \mathrm{K\,kbar^{-1}}$ for CeNiSnH, respectively. This difference is discussed in terms of hydrogen-induced modification of the balance between the Ruderman-Kittel-Kasuya-Yosida (RKKY) and the Kondo interactions. The μSR study demonstrates that the CeNiSnH and $CeNiSnH_{1.8}$ are on different sides of Doniach's dome. The behavior of the $CeNiSnH_{1.8}$ is interpreted as resulting from an increase of the hybridization between $4f$ and $5d$ states and a concomitant steep increase of the Kondo temperature upon applying pressure. In the quest for a quantum critical point, an estimated pressure of about 35 kbar is expected to suppress the magnetism in $CeNiSnH_{1.8}$.

DOI: 10.1103/PhysRevB.93.224424

I. INTRODUCTION

The intermediate valence behavior of many cerium-based intermetallics is well understood by invoking the existence of strong hybridization between the Ce $4f$ electrons and the conduction electrons. This interaction can be strongly influenced by the insertion of hydrogen into the lattice. Generally, hydrogenation induces both an expansion of the unit cell volume and a modification of the density of states at the Fermi level. Even transitions from a nonmagnetic state to an ordered magnetic state can be induced by H insertion [1]. For example, the hydrogenation of the intermediate valence indide CeNiIn produces the hydride $CeNiInH_{1.8}$ which exhibits ferromagnetic ordering below $T_C = 6.8$ K [2,3], i.e., the H insertion in CeNiIn induces a cerium valence transition from intermediate valence to the trivalent state. This effect results from the expansion of the unit cell volume V_m due to hydrogenation which increases the magnetic Ruderman-Kittel-Kasuya-Yosida (RKKY) interaction and decreases the Kondo interaction, the key ingredients whose competition explains most of the physical properties of the intermetallics based on cerium [4].

Another interesting example is the hydrogenation of the ternary stannide CeNiSn, a so-called Kondo semiconductor [5,6] that is classified as a strongly correlated $4f$-electron system. Exposed at 523 K to 1 MPa of hydrogen gas, this compound transforms into the hydride $CeNiSnH_{1.8}$ (H1.8) which decomposes at the same temperature but under low hydrogen pressure (5×10^{-3} MPa) into another hydride CeNiSnH (H1) [1,7,8]. The H1 hydride crystallizes, as CeNiSn, into an orthorhombic ε-TiNiSi type [6], whereas the H1.8 hydride belongs to a hexagonal ZrBeSi-type structure [7]. The increase of the unit cell volume due to hydrogenation is 2.6% for CeNiSnH and 8.0% for $CeNiSnH_{1.8}$.

As for CeNiIn, magnetic ordering is induced by the hydrogenation of CeNiSn. CeNiSnH is antiferromagnetic below $T_N = 4.5$ K whereas $CeNiSnH_{1.8}$ exhibits a ferromagnetic behavior below $T_C = 7.0$ K [1,7–9]. It is worth noting that the variation of volume induced by H insertion promotes magnetic ordering for both hydrides deriving from CeNiSn. Hydrogenation, which decreases the hybridization between the Ce $4f$ electrons and the conduction electrons, acts as "negative" pressure [10]. One should keep in mind that the temperature dependencies of the electrical resistivity and of the specific heat, for both hydrides, reveal a marked influence of the Kondo effect [9]: (i) The electrical resistivity of $CeNiSnH_{1.8}$ increases in a Kondo-like manner when the temperature decreases from 270 to about 25 K [7,9], and (ii) the analysis of the specific heat data in the paramagnetic range up to 20 K yields for $CeNiSnH_{1.8}$ an electronic coefficient $\gamma = 184\ \mathrm{mJ\,K^{-2}\,mol^{-1}}$ that is much larger than that corresponding to CeNiSnH ($\gamma = 39\ \mathrm{mJ\,K^{-2}\,mol^{-1}}$) [9]. Moreover, the magnetic entropy associated with the magnetic ordering of the two hydrides reaches only $0.54R\ln 2$, which is substantially reduced from $R\ln 2$, the value expected for a doublet ground state of the Ce^{3+} ion. This reduction of the magnetic entropy is interpreted as due to the Kondo interactions [11].

Magnetization under pressure experiments ($p < 10.8$ kbar) on the hydrides CeNiSnH and $CeNiSnH_{1.8}$ investigated the pressure dependence of their magnetic ordering temperature [10]. It is well known that the physical properties of the magnetic Kondo lattices, as described by Doniach's phase diagram, are strongly influenced by pressure [12]. It was shown that the magnetic properties of the hydrides derived from CeNiSn are differently influenced by the applied pressure p; with increasing p, the Néel temperature of CeNiSnH increases weakly from 4.77 to 5.01 K whereas the Curie temperature of $CeNiSnH_{1.8}$ decreases significantly from 7.16 to 5.30 K. Using electronic structure calculations for hydrides $CeNiSnH_x$ within the density functional theory, the authors have proposed an explanation for their magnetic properties:

(i) The density of states $n(E_F)$ at the Fermi level increases in the sequence CeNiSn $\rightarrow$ CeNiSnH $\rightarrow$ CeNiSnH$_{1.8}$, leading toward a transition from a Kondo semiconducting behavior to a magnetically ordered hydride; the corresponding density of states $n(E_F)$ amounts to 28, 49, and 81 Ryd^{-1} for CeNiSn, CeNiSnH, and CeNiSnH$_{1.8}$, respectively, and this increase of $n(E_F)$ is in agreement with that of the electronic coefficient γ (39 $\rightarrow$ 184 mJ K^{-2} mol^{-1}) as evidenced by specific heat measurements [9]; (ii) the Stoner products are then 0.56, 0.98, and 1.6 for CeNiSn, CeNiSnH, and CeNiSnH$_{1.8}$, respectively, and this increase explains the higher magnetic ordering temperature of CeNiSnH$_{1.8}$ than that observed for CeNiSnH; and (iii) finally, the occurrence of antibonding Ce-Ni states below the Fermi level for the CeNiSnH$_{1.8}$ hydride could be responsible for the decrease of its Curie temperature under applied pressure [10]. These calculations were recently confirmed by Aburto *et al.* [13].

In order to shed more light on the magnetic properties of CeNiSnH$_x$ and their pressure dependence ($p < 23$ kbar), we have performed muon spin rotation (μSR) experiments under pressure on CeNiSnH and CeNiSnH$_{1.8}$. The choice of such a technique is motivated by the fact that μSR (see Ref. [14] and references therein) was successfully employed in the past for the study of heavy fermions [15].

II. EXPERIMENT

In a typical μSR experiment, 100% polarized positive muons (spin $\frac{1}{2}$) are implanted into the sample, where they eventually come to rest at some crystallographic position; the muon spin performs a Larmor precession around the local magnetic field sensed at the stopping site; the muon decays (lifetime $\sim$2.2 ms) by emitting a positron, preferentially along the muon spin direction at the decay time. By recording for several millions of implanted muons the direction of the emitted positron as well as the time difference between the decay and the muon implantation, one can obtain information about the value of the local field at the muon site, field distribution, and spin dynamics, all those reflecting the magnitude and the fluctuating rate of the magnetic moments surrounding the muon.

The samples investigated in the present study, CeNiSnH and CeNiSnH$_{1.8}$, were prepared and characterized as previously described in Ref. [1]. The μSR experiments were performed at the Laboratory for Muon Spin Spectroscopy, Paul Scherer Institute (LMU, PSI), Villigen, Switzerland.

For measurements at *ambient pressure*, we have used the DOLLY instrument, located in the area πE1, in the temperature range 2–30 K. Data were recorded in zero field (ZF), weak transverse (with respect to the initial polarization of the muons) field (wTF), and longitudinal field (LF) field configurations. Two samples, A1 and A1.8, were prepared for the μSR experiments at ambient pressure, pressed into pellets of 10 mm in diameter and about 1.2 mm thickness, and mounted on a forklike sample holder in order to minimize any background signal.

The μSR *under pressure* experiments were performed up to about 23 kbar and down to 0.3 K using the General Purpose Decay-Channel Spectrometer (GPD) at the high energy muon beam line μE1. Two samples, P1 and P1.8, consisting of several pressed cylinders with a total length of about 13 mm and a diameter of 7 (5) mm for $p < 15$ kbar (15 kbar $< p <$ 23 kbar), were prepared and mounted in pressure cells. We used pressure cells made out of MP35N alloy [16] and Daphne oil was used as the liquid for transmitting the pressure. Pressure was applied at room temperature and estimated from *in situ* ac susceptibility measurements at low temperatures, from the shift of the superconducting transition temperature of a small piece of indium placed inside the p cell, close to the sample.

III. RESULTS AND DISCUSSIONS

A. CeNiSnH$_{1.8}$

μSR spectra recorded at ambient pressure, on sample A1.8, above and below the transition temperature $T_C \cong 6.8$ K, are displayed in Fig. 1. One can clearly distinguish the $T > T_C$ and $T < T_C$ temperature regions, from the time dependence of the polarization of the muon ensemble: It is weakly time dependent when the sample is in the paramagnetic state (the local fields at the muon sites are created by static nuclear magnetic moments and fast fluctuating electronic magnetic moments, both randomly oriented); it becomes strongly time dependent when the sample is in a ferromagnetic state (local fields dominated by the contribution of the ordered electronic moments). Moreover, for $T < T_C$, one can clearly observe two oscillations in the μSR spectra [see Fig. 1(b)], an indication of magnetically inequivalent muon stopping sites.

The μSR spectra were best fitted using

$$\begin{aligned} AP(t) = {} & A_{m1}\cos(2\pi\nu_1 t + \varphi 1)\exp(-\lambda_1 t) \\ & + A_{m2}\cos(2\pi\nu_2 t + \varphi 2)\exp(-\lambda_2 t) \\ & + A_{1/3}\exp(-\lambda_{1/3} t) + A_p P_{\mathrm{KT}}(t)\exp(-\lambda_p t), \end{aligned} \quad (1)$$

where A ($= A_{m1} + A_{m2} + A_{1/3} + A_p$) is the μSR asymmetry; the λ_i's are relaxation rates of the different signals and ν_i's are Larmor frequencies of the muon precession around the local magnetic fields, at low temperatures.

The first three terms on the right-hand side of Eq. (1) describe the pure magnetic regime ($A_p = 0$, $A_{m1} + A_{m2} + A_{1/3} = A$), where on average two thirds of the muons are subjected to a local field perpendicular to their initial spin polarization and will perform a Larmor precession with $\omega = \gamma B = 2\pi\nu$, while the remaining one third of the muons, $\frac{A_{m1}+A_{m2}}{2} = A_{1/3}$, will sense a local field parallel to their spin and therefore will not precess. However, if the magnetic field at the muon site is not static, the fluctuating field components perpendicular to the muon spin polarization can induce transitions between the two spin states of the muon and produce relaxation. Therefore, a nonzero $\lambda_{1/3}$ is a clear signature of fluctuating magnetic moments in the magnetic ordered state.

The last term in Eq. (1) describes the paramagnetic regime ($A_p = A$, $A_{mi} = A_{1/3} = 0$), with a depolarization of the muon ensemble taking place via two channels. The first depolarization channel is due to the field distribution created by the static (for the time window of the μSR experiments) and randomly oriented nuclear moments, leading to the so-called Kubo-Toyabe depolarization function $P_{\mathrm{KT}}(t) = \frac{1}{3} + \frac{2}{3}(1 - \sigma^2 t^2)\exp(-\frac{\sigma^2 t^2}{2})$. The second depolarization channel

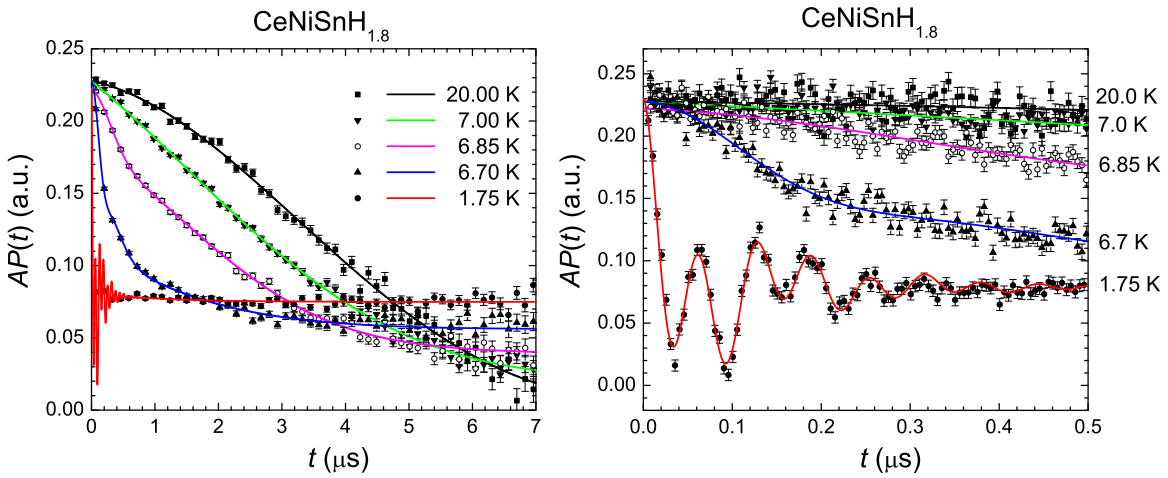

FIG. 1. μSR spectra recorded at selected temperatures above and below T_C. Left: long time scale; right: small time scale. Lines are fits of Eq. (1) to the data.

originates from μ^+ fluctuations induced by the fast fluctuating electronic magnetic moments. Therefore, at temperatures above the magnetic transition, $AP(t) = A_p P_{KT}(t)\exp(-\lambda_p t)$ was used to fit the μSR data. In the vicinity of the transition temperature the entire Eq. (1) is used.

B. $CeNiSnH_{1.8}$ in the paramagnetic state, $T > T_C$

The depolarization rate σ from Eq. (1) was found to be practically temperature independent, $\sigma \cong 0.2\ \mu s^{-1}$. It is related to the second moment of the field distribution created by the nuclear moments at the muon site, and corresponds to a width of a field distribution of about 2.3 G. Its value is a few times larger than that found for CeNiSn [17], which is conceivable, since the natural abundances of the CeNiSn's constituent elements having nonzero nuclear moments are small: 7.65% for ^{117}Sn, 8.68% for ^{119}Sn, and 1.25% for ^{59}Ni, while ^{1}H with spin $\frac{1}{2}$ has almost 100% abundance.

The temperature dependence of the relaxation rate in the paramagnetic phase λ_p, close to the transition, is plotted in Fig. 2. The inset in Fig. 2 depicts the longitudinal field (LF) dependence of the relaxation rate, measured at 7.5 K. Both dependencies are rather similar to those obtained for CeNiSn [17]. However, a quantitative comparison is not possible as the authors of Ref. [17] omitted the contribution of the nuclear moments in their fitting procedure. The increase of λ_p with the decrease of temperature is ascribed, in our case, to the buildup of correlated fluctuations between the fluctuating Ce electronic moments prior to the magnetic transition. Those correlations are sharply suppressed by applying a relatively small (30 G) longitudinal field, i.e., they give a contribution to the second moment of the field distribution of the same order of magnitude as that given by the nuclear moments. One can clearly observe that $\lambda_p(B)$ is not suppressed to zero at large fields but to a finite value which corresponds more or less to the asymptotic value of $\lambda_p(T)$ at high temperatures, where the spins have uncorrelated fluctuations.

C. $CeNiSnH_{1.8}$ in magnetic state, $T < T_C$

The temperature dependencies of ν_1 and ν_2 are displayed in Fig. 3. They provide a quite precise estimation of the transition temperature, and reflect the temperature dependence of the order parameter. The lines in Fig. 3 are fits to the data using a phenomenological model:

$$\nu_i(T) = \nu_i(0)[1 - (T/T_C)^a]^\beta. \quad (2)$$

With the exception of $\nu_i(0)$, all the other parameters were kept identical for the fit of the two $\nu_i(T)$ curves. The value of the transition temperature at ambient pressure is $T_C \cong 6.8$ K. We note that the values of α (=3.15) and β (=0.58) are not reliable due to the lack of experimental points in the vicinity of the magnetic transition.

The temperature dependence of λ_1 and λ_2, not shown here, is practically flat with $\lambda_1 \cong 6.6\ \mu s^{-1}$ and $\lambda_2 \cong 11.4\ \mu s^{-1}$. On the other hand, $\lambda_{1/3}$ is very small and close to 0.01 μs, indicating that the magnetic ordering is quasistatic within the time window of the μSR experiment.

For the samples in the pressure cell, another term, $A_{cell}P_{cell}(t)$, describing the μSR signal of the muons stopped in the pressure cell's walls, should be added to Eq. (1): $P_{cell}(t) =$

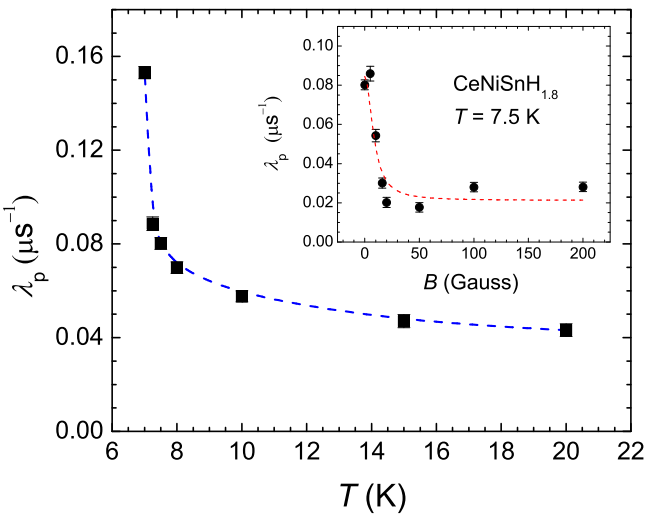

FIG. 2. $\lambda_p(T)$ dependence. The inset shows the $\lambda_p(B)$ dependence recorded at 7.5 K. The dotted lines are guides for the eye.

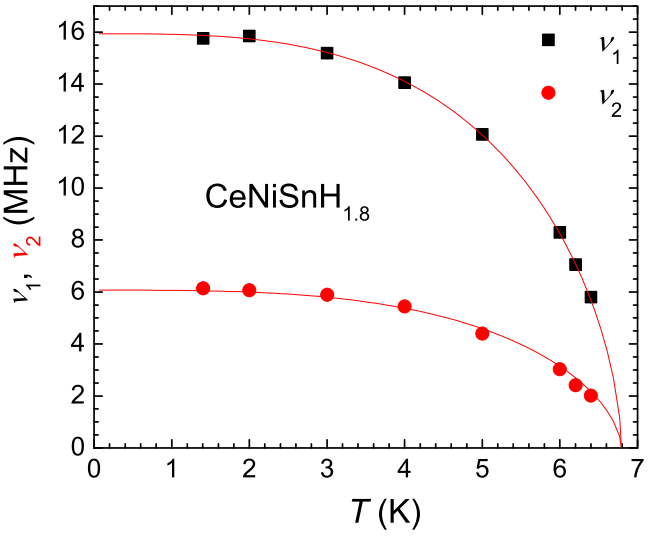

FIG. 3. Temperature dependence of the spontaneous muon spin frequencies ν_1 and ν_2. The lines represent a fit as described in the text.

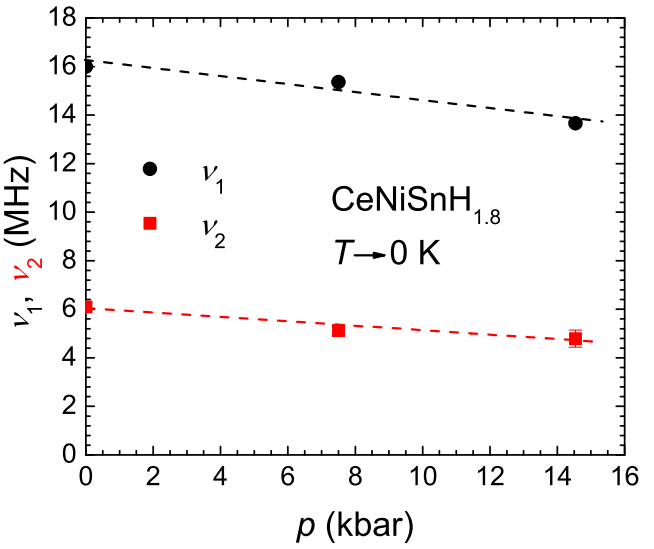

FIG. 5. Pressure dependence of $\nu_1(T \rightarrow 0)$ and $\nu_2(T \rightarrow 0)$. Dotted lines are guides to the eye.

$P_{\mathrm{KT,cell}}(t)\exp(-\lambda_{\mathrm{cell}}t)$. The temperature dependence of both σ_{cell} and λ_{cell} are known from μSR experiments on empty p cells [18].

The temperature dependence $\nu_i(T)$ obtained from fits of the μSR spectra recorded at 14.5 kbar is shown in Fig. 4. The red lines are fits of the data using the phenomenological formula described above, with the same α and β parameters obtained from the ambient pressure data. The dashed blue lines indicate, for comparison, the fits of the experimental data recorded at ambient pressure.

The pressure dependence of the ν_i ($T = 1$ K) is presented in Fig. 5 and the pressure dependence of the transition temperature is shown in Fig. 6. Our experiment clearly indicates a reduction, with an increase of the applied pressure, of the ordered moment in CeNiSnH$_{1.8}$ and confirms the $T_C(p)$ dependence found by Fernandez and co-workers [10]. A linear fit of the data yields an average of $\frac{d\nu}{dp} = -0.16$ MHz kbar^{-1} and $\frac{dT_C}{dp} = -0.17$ K kbar^{-1}. The maximum pressure obtained in our experiments, $\cong$23 kbar, was not enough to suppress the magnetic ordering in this compound.

The data presented in Fig. 6 were obtained from temperature scans across the magnetic transition, in a weak transverse field of 50 G. Above the temperature of the magnetic transition, the sample is in a paramagnetic state and therefore all the muons' spins perform an identical Larmor precession around the applied field. At temperatures below the magnetic transition

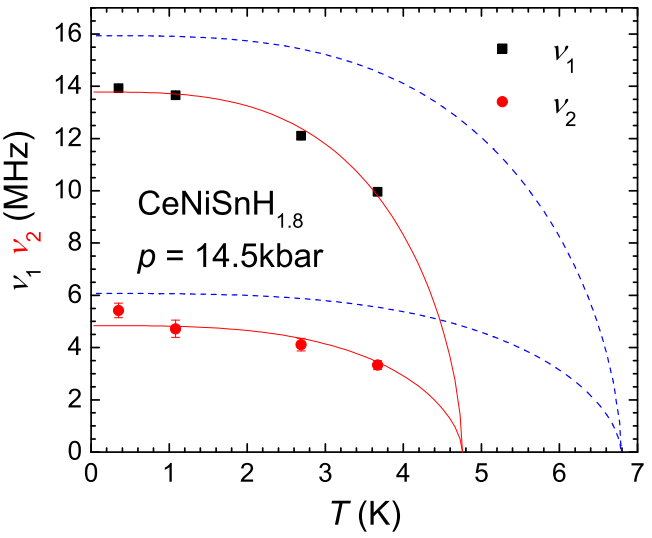

FIG. 4. Temperature dependence of the Larmor frequencies ν_i at 14.5 kbar. The continuous (red) line represents the fit described in the text and the dotted (blue) lines show the $\nu_i(T)$ dependency at ambient pressure.

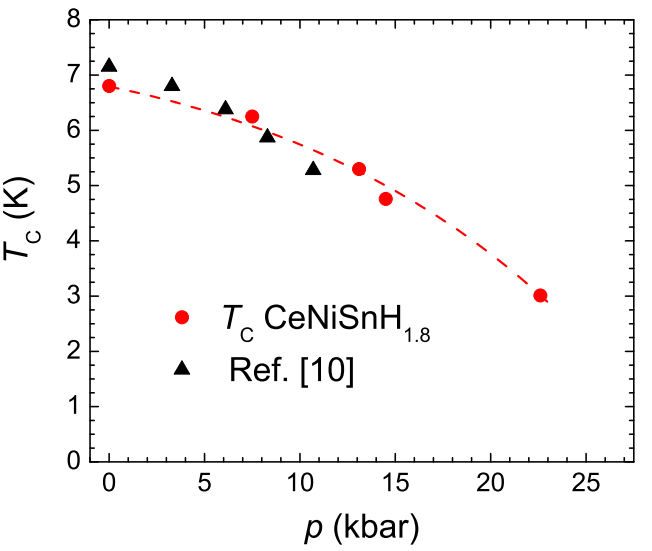

FIG. 6. Pressure dependence of the transition temperature T_C (red points) for CeNiSnH$_{1.8}$. The triangles show results obtained from macroscopic measurements [10]. The dotted line is a guide for the eye.

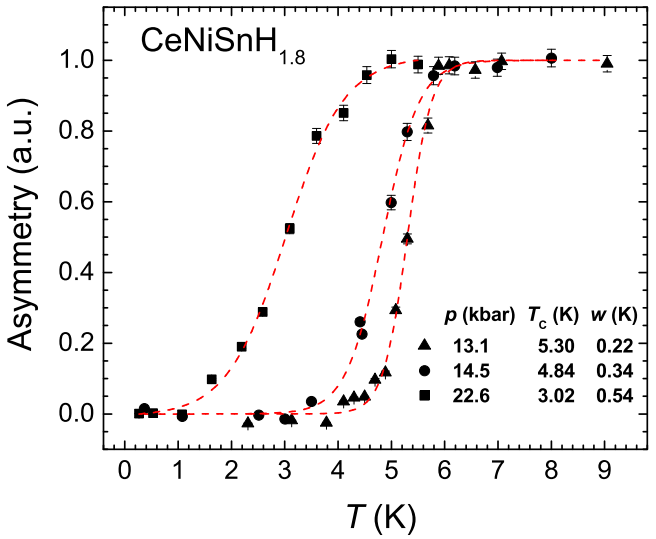

FIG. 7. Temperature dependence of the normalized amplitude of the 50 G signal, measured across the magnetic transition. The dotted lines are fits of Eq. (3) to the data.

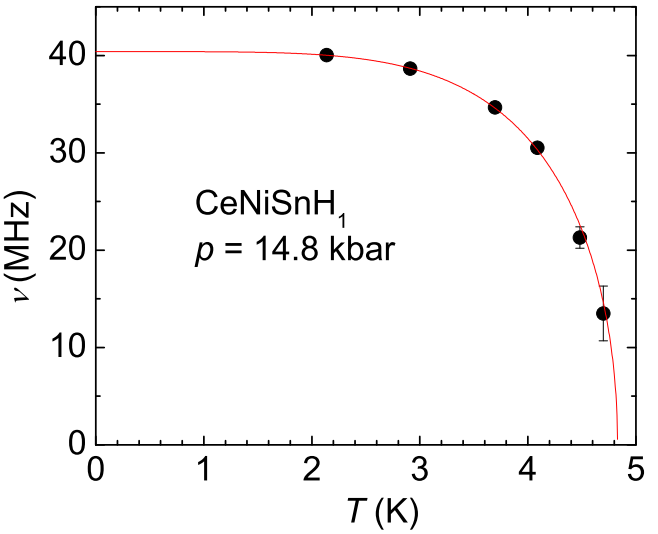

FIG. 9. Temperature dependence of the Larmor frequency ν, for the P1 sample, at 14.8 kbar. The continuous (red) line is a fit of Eq. (2) to the $\nu(T)$ data.

temperature, the local fields created by the ordered magnetic moments are much larger than the applied 50 G and thus the 50 G signal is lost. Keep in mind that the muon's Larmor precession frequency is related to the local field by $2\pi\nu = \gamma_\mu B$, with $\gamma_\mu/2\pi \cong 0.013\,55$ MHz/G, so a frequency $\nu = 5$ MHz, for example, corresponds to a local field at the muon site of about 370 G.

The temperature dependence of the normalized amplitudes of the 50 G signal corresponding to the sample, measured at selected pressures, is presented in Fig. 7. The signal was normalized and the p-cell signal was subtracted in order to facilitate the comparison between the different pressures. As mentioned before, two different p cells were used, one for low p (up to 15 kbar) and the other one for the high p (up to 23 kbar) μSR experiments, with different inner diameters.

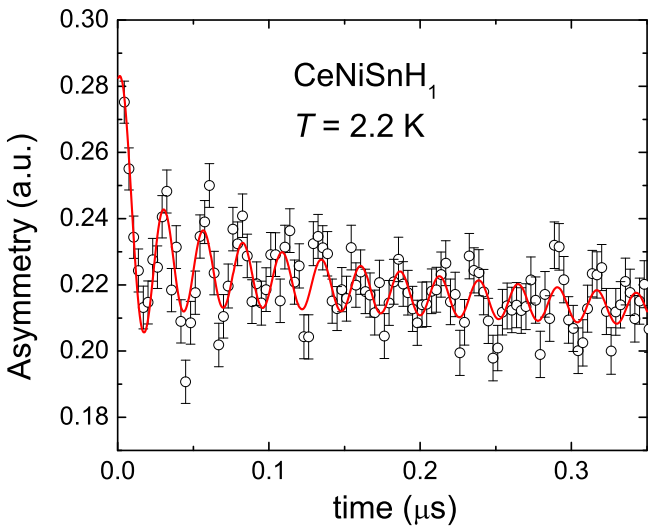

FIG. 8. μSR spectrum recorded at $T < T_N$ for CeNiSnH. The line represents the fit of the μSR data (see text).

The experimental points were fitted using a phenomenological function

$$A(T) = A_1 - A_2/\{1 + \exp[(T - T_m)/w]\}, \qquad (3)$$

which provides T_m the transition temperature, A_1 the total asymmetry, A_2 the asymmetry of the sample, and a measure of the width of the transition, w (a small value of w corresponds to a sharp magnetic transition).

D. CeNiSnH

Data solely obtained on the P1 samples, i.e., the cylindrical sample measured inside the p cell, are presented here. Indeed, a thorough analysis of the experimental results for the A1

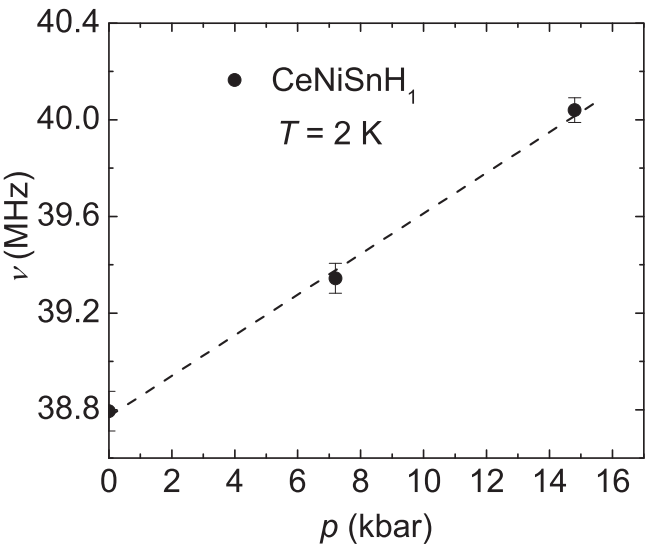

FIG. 10. Pressure dependence of the Larmor frequency $\nu(T = 2\text{ K})$ for the P1 sample. The dotted line is a guide for the eye.

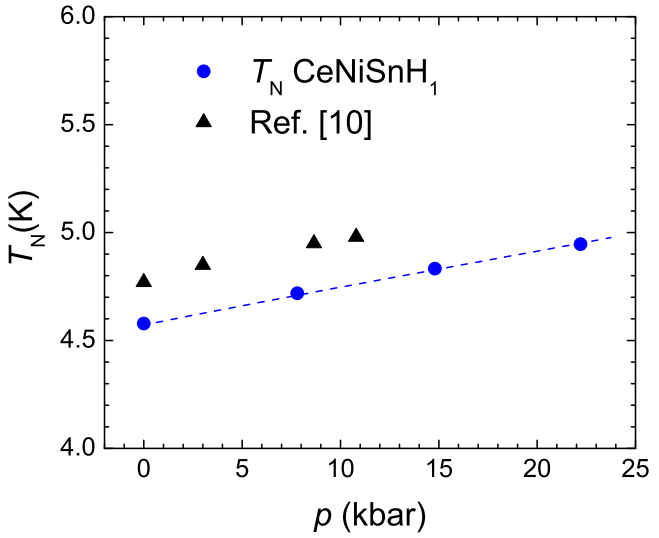

FIG. 11. Pressure dependence of T_N for CeNiSnH. The dotted line is a guide for the eye.

sample, the pellet used for the ambient pressure experiment, has shown that the A1 sample was in fact a mixture of $CeNiSnH_1$ and $CeNiH_{1.8}$, a fact confirmed afterwards by a reinvestigation of its crystal structure. We note that this finding is still an important point to mention since it shows the power of μSR in detecting/solving phase-separation issues. Therefore, all the information concerning CeNiSnH is obtained from μSR under pressure experiments (at ambient and high pressures), performed on the P1 sample, i.e., from the sample mounted inside the pressure cell. Figure 8 presents a μSR spectrum recorded at ambient pressure, below the transition temperature $T_N = 4.6$ K. The best fit of the μSR spectra was obtained using

$$\begin{aligned} AP(t) = {} & A_{m1} J_0(\gamma_\mu B_{\max} t) c \exp(-\lambda_1 t) + A_{1/3} \exp(-\lambda_{1/3} t) \\ & + A_p P_{\mathrm{KT}}(t) \exp(-\lambda_p t) \\ & + A_{\mathrm{cell}} P_{\mathrm{KT,cell}}(t) \exp(-\lambda_{\mathrm{cell}} t), \end{aligned}$$

where $J_0(\gamma_\mu B_{\max} t)$ is the Bessel function of zero order. For the meaning of the other terms, see above. A Bessel fit function is usually taken as the signature of an incommensurate magnetism (see Ref. [18] and references therein). Neutron scattering experiments would be needed in order to confirm the incommensurability of the magnetic cell.

The temperature dependence of the fitted frequency, recorded at 14.8 kbar, is shown in Fig. 9. The red line is a fit of Eq. (2) to the $\nu(T)$ data.

The pressure dependence of $\nu(T = 2\,\mathrm{K})$ is plotted in Fig. 10 and the pressure dependence of T_N, obtained from temperature scans across the magnetic transition in a weak transverse field of 50 G, is plotted in Fig. 11, together with data obtained from macroscopic measurements [10]. The pressure dependence is weaker and opposite, i.e., positive, for both ν and T_N, in the case of CeNiSnH, $\frac{d\nu}{dp} = 0.084$ MHz kbar^{-1} and $\frac{dT_N}{dp} = 0.016$ K kbar^{-1}, compared with what was obtained for $CeNiSnH_{1.8}$.

In Fig. 12 we propose a tentative position of the three investigated $CeNiSnH_x$ compounds in Doniach's diagram [19] on the basis of the above reported pressure dependencies of their magnetic transition temperature. As can be seen from Fig. 12 (right), the Néel temperature of the H1 compound is much less sensitive to the applied pressure than the Curie temperature of the H1.8. They not only evolve in opposite directions, in good agreement with the prediction of Doniach's diagram, but the observed pressure dependence is also in agreement with the expected lower sensitivity to pressure of the antiferromagnetic-type magnetic order temperature. According to this diagram, the observed increase of T_N with the applied pressure for CeNiSnH is mostly due to the reinforcement of the RKKY exchange interactions between the Ce atoms. Indeed, the insertion of hydrogen within the lattice is expected to affect the RKKY interaction via its dependence on both the interatomic distances and the density of states at the Fermi level. The negative pressure dependence of $CeNiSnH_{1.8}$ is suggestive of the presence of an increase of the hydridization between the $4f$ and $5d$ states and the concomitant increase in the Kondo interactions.

Even though it is known that hydration leads to an increase of the sample's volume, i.e., acts as negative pressure, it is not

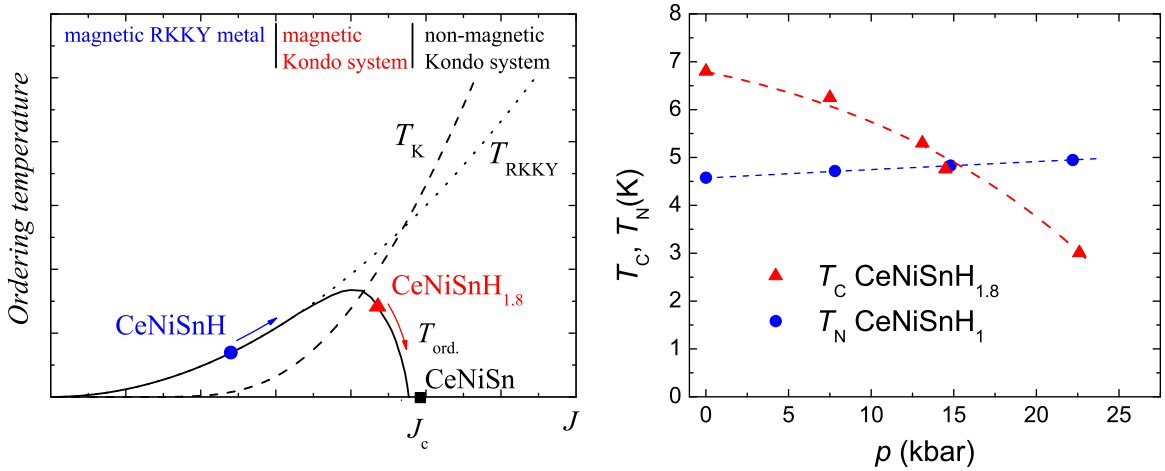

FIG. 12. Left: Schematic representation of Doniach's phase diagram indicating the relative position of the $CeNiSnH_x$ compounds ($x = 0, 1$, and 1.8). Right: The pressure dependence of the Néel and Curie temperature of the H1 and H1.8 hydrides, respectively. Dotted lines are guides for the eyes.

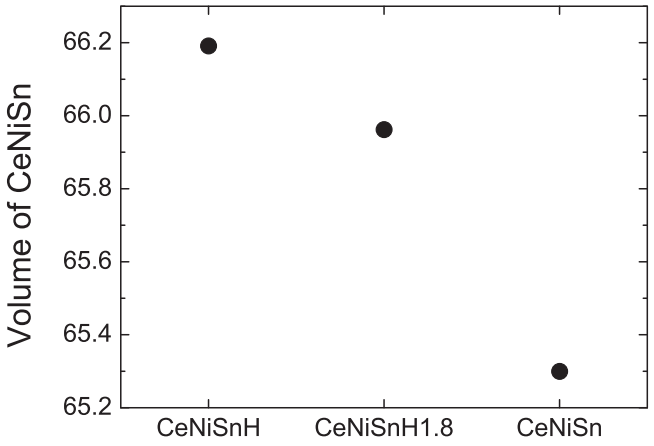

FIG. 13. Sum of the Wigner-Seitz atomic cell volume of the metallic Ce-Ni-Sn atoms in $CeNiSnH_x$ compounds.

straightforward to explain why for the H1 sample the negative pressure effect induced by hydration is larger than for the H1.8 sample. Looking at the Wigner-Seitz volumes associated with the different atoms in the structure, we have found that only the volume of the metallic atoms Ce-Ni-Sn (obtained after the subtraction of the hydrogen's volume from the unit cell's volume) decreases from H1 to H1.8 and H0 samples, as shown in Fig. 13.

IV. CONCLUSION

This study demonstrates the importance of hydrogen as a probe to modify the magnetic properties of Ce containing compounds. The effect of hydrogen on Ce magnetism is large and most probably cannot be restricted to a chemical pressure effect since the hydrogen insertion also introduces an additional electron to the system. Concerning the RKKY interactions, both the electron density at the Fermi level and the interatomic distances are expected to play a major role in the hydrogen-induced modification of the magnetic ground state. It is worth recalling that the presence of hydrogen in the Ce atomic environment of Ce TX compounds is known to significantly change the hybridization of the Ce $4f$-$5d$ electronic states [1]. Whereas the CeNiSn compound is known to present typical semiconductor Kondo behavior, its hydrides H1 and H1.8 are exhibiting magnetic ordering. CeNiSnH behaves as antiferromagnetic material with dominant RKKY exchange interactions. On the contrary, $CeNiSnH_{1.8}$ orders ferromagnetically at 7.0 K. The present μSR spectroscopic investigation shows that both magnetic order temperatures are sensitive to the applied pressure but in opposite directions: negative $\frac{dT_C}{dp} = -0.17\ \mathrm{K\,kbar^{-1}}$ of $CeNiSnH_{1.8}$ and positive $\frac{dT_N}{dp} = 0.016\ \mathrm{K\,kbar^{-1}}$ for CeNiSnH. While for CeNiSnH, an estimation of the critical pressure is not obvious, a pressure of about 35 kbar might suppress the magnetism in $CeNiSnH_{1.8}$.

The opposite behavior of T_N and T_C of the H1 and H1.8 compounds has been analyzed in light of Doniach's diagram. It is found that the balance of the RKKY and Kondo interactions is modified upon hydrogen insertion.

On the other hand, application of pressure on the $CeNiSnH_x$ hydrides favors, via a pure volume effect, a progressive modification of the balance between the RKKY and Kondo interaction, offering also the possibility of locating the samples on Doniach's diagram. In the case of the H1.8 compound, the steep increase of T_K appears to be the dominant factor, thus leading to the rapid decrease of the Curie temperature upon applying pressure.

The μSR experiments on CeNiSnH and $CeNiSnH_{1.8}$ confirm that the investigated compounds are on different sides of Doniach's dome and indicate that higher pressures are needed in order suppress the magnetism in these compounds in the quest for a quantum critical point. Further studies at higher pressures would be very interesting to search for the existence of a quantum critical point and to investigate the physics at the vicinity of such remarkable points.

ACKNOWLEDGMENTS

C.R. acknowledges partial financial support from The Sectoral Operational Programme Human Resources Development, Contract POSDRU 6/1.5/S/3, "Doctoral studies: through science towards society." D.A., R.D., and C.R. acknowledge partial financial support from Romanian UEFISCDI Project No. PN-II-ID-PCE-2011-3-0583 (85/2011). Part of this work was performed at the Swiss Muon Source, Paul Scherrer Institut, Villigen, Switzerland.

[1] B. Chevalier, M. Pasturel, J.-L. Bobet, R. Decourt, J. Etourneau, O. Isnard, J. Sanchez Marcos, and J. Rodriguez Fernandez, J. Alloys Compd. **383**, 4 (2004).
[2] B. Chevalier, M. L. Kahn, J.-L. Bobet, M. Pasturel, and J. Etourneau, J. Phys.: Condens. Matter **14**, L365 (2002).
[3] K. Shashikala, A. Sathyamoorthy, P. Raj, S. K. Dhar, and S. K. Malik, J. Alloys Compd. **437**, 7 (2007).
[4] G. R. Stewart, Rev. Mod. Phys. **73**, 797 (2001).
[5] A. Hiess, I. Zobkalo, M. Bonnet, J. Schweizer, E. Lelievre-Berna, F. Tasset, Y. Isikawa, and G. H. Lander, Physica B **230**, 687 (1997).
[6] A. Hiess, I. Zobkalo, M. Bonnet, J. Schweizer, E. Lelièvre-Berna, F. Tasset, Y. Isikawa, and G. H. Lander, J. Phys.: Condens. Matter **9**, 9321 (1997).
[7] B. Chevalier, J.-L. Bobet, M. Pasturel, E. Bauer, F. Weill, R. Decourt, and J. Etourneau, Chem. Mater. **15**, 2181 (2003).
[8] V. A. Yartys, B. Ouladdiaf, O. Isnard, O. Y. Khyzhun, and K. H. J. Buschow, J. Alloys Compd. **359**, 62 (2003).
[9] B. Chevalier, M. Pasturel, J.-L. Bobet, J. Etourneau, O. Isnard, J. Sanchez Marcos, and J. Rodriguez Fernandez, J. Magn. Magn. Mater. **272–276**, 576 (2004).
[10] J. Rodriguez Fernandez, S. F. Matar, D. P. Rojas, L. Torralbo-Campo, and B. Chevalier, J. Phys.: Condens. Matter **21**, 305601 (2009).
[11] J. A. Blanco, M. de Podesta, J. I. Espeso, J. C. Gomez Sal, C. Lester, K. A. McEwen, N. Patrikios, and J. Rodriguez Fernandez, Phys. Rev. B **49**, 15126 (1994).

[12] J. Larrea, M. B. Fontes, A. D. Alvarenga, E. M. Baggio-Saitovitch, T. Burghardt, A. Eichler, and M. A. Continentino, Phys. Rev. B **72**, 035129 (2005).
[13] A. Aburto and E. Orgaz, Phys. Rev. B **75**, 045130 (2007).
[14] A. Yaouanc and P. Dalmas de Réotier, *Muon Spin Rotation, Relaxation, and Resonance* (Oxford University Press, Oxford, UK, 2011).
[15] A. Amato, Rev. Mod. Phys. **69**, 1119 (1997).
[16] I. R. Walker, Rev. Sci. Instrum. **70**, 3402 (1999).
[17] A. Yaouanc, P. Dalmas de Réotier, P. C. M. Gubbens, A. M. Mulders, and Y. Isikawa, Physica B **289-290**, 28 (2000).
[18] D. Andreica, Ph.D. thesis, ETH Zurich, 2001, doi:10.3929/ethz-a-004171645.
[19] S. Doniach, Physica B **91**, 231 (1977).